Environmental Engineering and Management Journal

November 2019, Vol.18, No. 11, 2533-2541
http://www.eemj.icpm.tuiasi.ro/; http://www.eemj.eu

"Gheorghe Asachi" Technical University of Iasi, Romania

EXPERIMENTAL RESEARCH ON SPRAY COOLING FEATURES OF PRESSURE NOZZLE IN HUMIDIFICATION CHAMBER

Xiaoqing Huang[1,2*], Dongliang Zhang[1], Xu Zhang[3]

[1]College of Energy and Power Engineering, Nanjing Institute of Technology, Nanjing 211167, China
[2]School of Energy and Environment, Southeast University, Nanjing 210096, China
[3]Institute of HVAC &Gas, Tongji University, Shanghai 201804, China

Abstract

The normal operation of spray humidification air cooler hinges on the good contact between droplets and air in the humidification chamber. The spiral pressure nozzle was chosen for the experiment on inlet air spray cooling. During the experiment, the spray cooling performance and atomization features were examined, and the cooling effects of different nozzle layouts were compared.Through the analysis of heat and mass transfer, the critical pressure of the spiral pressure nozzle was determined, and the relevant phenomenon was explained based on the energy balance relationship in droplet atomization. Meanwhile, the cooling effect fitting correlation was acquired with evaporative cooling being the major cooling mechanism. The comparison between different nozzle layouts revealed that the cooling effect of row spacing: 500mm is superior to that of row spacing: 1,000mm under the condition of the same $\Delta T \cdot L$. In this way, the critical pressure and optimal layout of the spiral pressure nozzle in the humidification chamber were discovered.

Keywords: atomization features, fitting correlation of cooling effect, spray humidification air cooler, spiral pressure nozzle

Received: March, 2019; Revised final: June, 2019; Accepted: July, 2019; Published in final edited form: November, 2019

1. Introduction

Coal-fired thermal power accounts for 42% of electricity generated in China, the largest share of any power source. Thus, it is unsurprising that thermal power generation industry is the biggest consumer of water in the country (Wu and Qi, 2001). However, the major coal-production regions in China are concentrated in the northern part, which is known for the scarcity of water resources. The water shortage is worsened by the growing demand of domestic, agricultural and industrial water, putting enormous pressure on China's water resources supply and environmental protection.

Air cooling is one of the most effective technologies to save water in thermal power plants, but it is much costlier than water cooling and heavily influenced by the ambient temperature. The problem is particularly acute in the summer. Under the high ambient temperature, the outlet temperature of the air cooler may exceed the allowed range, push up the back pressure of gas turbine, and endanger the cooling system and the power plant.

To solve this problem, evaporative cooling has been proposed to enhance the air side heat transfer of the air cooler. The typical applications with evaporative cooling include hybrid (dry/wet) air cooler, deluge-type air cooler (Wu, 2007) and humidification air cooler. Among them, the humidification air cooler is further divided into packing humidification air cooler and spray humidification air cooler. As the name suggests, the spray humidification air cooler cools down the inlet air by spraying water vapour through a nozzle. Because of low initial investment, high rate of return and relatively simple system, the spray humidification air

*Author to whom all correspondence should be addressed: e-mail: hxq-101@163.com; Phone: 86-86118355; Fax: 86-86118355

cooler was selected as the object of this research (Bal, et al., 2018; Chen et al., 2013; Kutscher and Costenaro, 2002; Li et al., 2016). A new humidification air cooling system was introduced and compared to the spray cooling (Zeng et al., 2019).

Based on shape and spray mode, air cooler nozzles roughly fall into the following categories: pressure atomizing nozzle, rotary atomizing nozzle, dual-fluid atomizing nozzle, ultrasonic atomizing nozzle, and percussive atomizing nozzle (Bishnoi and Sinha, 2018; Camaraza-Medina et al., 2018; Dai et al., 2018; Lefebvre, 1989). The pressure atomizing nozzle stands out as the most popular nozzle in the fields of spray cooling and fire control.

The TF nozzles are one of the most popular pressure nozzles in engineering. With a fixed spray angle, this series of nozzles will not witness the reduction in the spray cone angle under high injection pressure. Besides, the TF nozzles are rarely blocked in operation, because they are well integrated with no separate element inside. Therefore, the author selected the TF6 pressure atomizing nozzle (BETE, flow number 3.18, and the operating pressure range 0.05~2 MPa) for inlet air spray cooling.

2. Literature review

Over the years, spray cooling has often been studied in association with spray fire suppression. From both practical and theoretical perspectives, Atreya et al. (1999), Grant et al. (2000), Lentati and Chelliah (1998), Jones and Nolan (1995), Sardqvist and Holmstedt (2001) explored the interaction between spray and flame, and disclosed the effect of nozzle pressure on temperature distribution and gas concentration in the fire area. Similarly, Prasad et al. (1998; 2002) and Keramida et al. (2000) numerically analysed how spray impacts the temperature distribution in the fire area.

Back et al. (2000), Hansen and Back (2001) performed experiments on spray fire suppression in confined and open spaces, identified the relationship between spray droplet diameter and fire suppression effect, and established the quasi-static model of spray fire suppression in confined spaces. Jukka (2002) established the transient calculation model for spray fire suppression in well-ventilated spaces, utilized the model to capture the temporal variation of gas temperature, gas density, gas composition and water mist concentration, and verified the effectiveness of the model using experimental data.

Probing into spray suppression of methane gas fire, Shimizu et al. (2001) obtained the relationship between fire intensity and spray volume, and revealed the influence of spray droplet diameter on fire suppression. Li et al. (2015) introduced evaporative cooling systems in some other areas. Lorenzini (2006), Lorenzin and Saro, (2013; 2016), Wrachien and Lorenzin (2012) investigated droplet dynamics in spray irrigation and analysed the energy balance during droplet atomization. Lorenzini and Saro (2016) analysed water droplet evaporation through a theoretical-numerical model.

As a result, it is necessary to study the features of spray cooling independently. In this research, experiments are arranged to disclose the relationship between nozzle pressure and spray cooling effect, and to improve the nozzle arrangement in the humidification chamber.

3. Experimental

3.1 Experimental setup

Our spray cooling system comprises a high-temperature flue system, a ventilation system and a spray system (Fig. 1). The high-temperature flue system consists of a circulating fan, a hot air stove, a wind pipe and a measuring section; the ventilation system is composed of an induced draft fan, an exhaust fan, a fan controller, a wind pipe, an air sampler and a measuring section; the spray system includes a water tank, a high-pressure water pump, several nozzles, a water receiver and a measuring section.

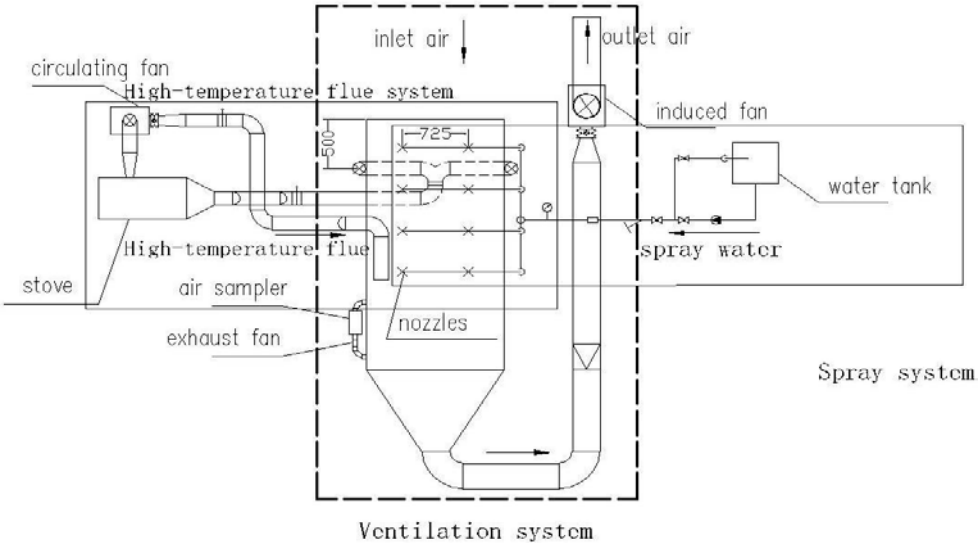

Fig. 1. Schematic of spray cooling system (unit: mm)

The experimental section is shaped as a rectangular box (2,500mm×1,450mm×800mm). On top of the section, the nozzles were arranged in four rows with a row spacing of 500mm. In each row, the nozzles were separated by an interval of 725mm. The water receiver was placed at the bottom of the section. As shown in Fig. 2, the nozzles are TF6 spiral pressure nozzles. With a male thread diameter of 1/4-inch, each nozzle can create a solid cone spray at the angle of 90°. The main measured parameters and measuring instruments are listed in Table 1. Data collection was carried out by Fluke DAQ every 10s. The author tested the effects of TF6 nozzles in different layouts by individually opening the nozzles in row 1 and row 2 (hereinafter referred to as 1/2 TF6) and the nozzles in row 1 and row 3 (hereinafter referred to as 1/3 TF6). In total, the experiment covers 7 working conditions of 1/2 TF6 (different inlet air temperature differences between dry-bulb and wet-bulb temperatures), and 2 working conditions of 1/3 TF6.

Fig. 2. Schematic of TF6 nozzle

3.2 Experimental theory

The spray cooling effect of the air side was calculated following the principles of heat and mass transfer. In essence, the heat transfer and the mass transfer were respectively driven by temperature difference of the air and partial pressure difference of the water vapour.

If we denote the temperature difference of the air as *dT*, the water content difference as *dm*, and the infinitesimal contact area between the air and water vapour as *dA*, the sensible heat transfer can be defined as:

$$dQ_x = -Gc_p dT = h(T - T_b)dA \quad (1)$$

where G is the mass flow of the air in contact with water vapour (kg/s); c_p is the specific heat capacity of the air (J/(kg·℃)); h is the sensible heat transfer coefficient of the air-water interface (W/(m2·℃)); T is the main air temperature (°C); T_b is the boundary layer air temperature (°C).

The moisture transfer amount can be defined as:

$$dW = Gdm = h_{mp}(P_q - P_{qb})dA \quad (2)$$

where: h_{mp} is the moisture transfer coefficient of the air-water interface, calculated in accordance with the partial pressure difference of water vapour (kg/(N·s)); P_q and P_{qb} are the partial pressures of water vapour in the main air and in the boundary layer, respectively (Pa).

Table 1. Main experimental parameters and instruments

System	***Measurement parameters***	***Instrument***	***Measuring range and precision***
High-temperature flue system	Supply flue temperature	Thermal resistance temperature detector	-70~500℃ 0.5%FS
	Return flue temperature	Thermal resistance temperature detector	-70~500℃ 0.5%FS
	Dynamic pressure of flue pipeline	Pitot tube	2~70 m/s 0.25%FS
Ventilation system	Inlet air temperature	Thermograph	-50~70℃ 0.5%FS
	Outlet air temperature	Normal temperature thermo coupler×5	-50~70℃ 0.5%FS
	Duct dynamic pressure	Pitot tube	2~70 m/s 0.25%FS
	Air sampler dry bulb temperature	Thermometer×2	0~50℃; 50~100℃ 0.5%FS
	Air sampler wet bulb temperature	Thermometer	0~50℃ 0.5%FS
Spray system	Spray water temperature	Thermometer	0~50℃ 0.5%FS
	Spray water flow	Turbine flow meter LWGY-25 and digit expression meter	0~10 m^3/h 0.2%FS
	Spray system pressure	Pressure meter YB150	2.5 MPa accuracy 0.4
	Droplet diameter	Malvern spraytec particle size analyzer	0.1 μm~2000 μm ±1%

The moisture transfer can be described by Eq. 3 because the partial pressure difference of water vapour can be replaced by product of the water content difference and moisture transfer coefficient within a small temperature range:

$$dW = h_{md}(m - m_b)dA \quad (3)$$

where h_{md} is the moisture transfer coefficient of the air-water interface, calculated in accordance with the water content difference (kg/(m^2·s)); m and m_b are the moisture in the main air and in the boundary layer, respectively (kg/kg).

The latent heat transfer rate can be calculated with the Eq. (4).

$$dQ_q = rdW = rh_{md}(m - m_b)dA \quad (4)$$

where: r is the latent heat of vaporization at the temperature of T_b (J/kg).

Eq. (5) can be obtained as the total heat transfer rate $dQ_z=dQ_x+dQ_q$.

$$dQz = \left[h(T - T_b) + rh_{md}(m - m_b)\right]dA \quad (5)$$

4. Results analysis

4.1. Analysis of heat transfer and mass transfer

In the spray cooling experiment, the heat transfer and mass transfer were investigated by opening the TF6 nozzles in row 1 and row 2 (row spacing: 500mm). Out of all 7 working conditions, the second working condition (hereinafter referred to as 1/2 TF6 WC2) was taken as the example for detailed analysis. The nozzle pressure was controlled at 10 values, namely 0.05, 0.07, 0.10, 0.20, 0.30, 0.50, 0.70, 1.00, 1.50 and 2.00MPa.

Initially, the dry-bulb temperature and the wet-bulb temperature of air at the chamber inlet were 79.2 °C and 36.4 °C, respectively (Fig. 3). Then, the dry-bulb temperature decreased substantially with the increase in nozzle pressure and water flow. The dry-bulb temperature approached the wet-bulb temperature when the nozzle pressure reached 0.70MPa. As the nozzle pressure increased, the dry-bulb temperature was in gentle decline and closed in on the wet-bulb temperature.

The heat and mass transfer processes in 1/2 TF6 WC2 is illustrated in Fig. 4. The sensible heat transfer (Q_x) decreased at first as the nozzle pressure increased, and achieved the balance when the nozzle pressure reached 0.70MPa, showing a similar trend to that of the dry-bulb temperature. The latent heat transfer (Q_q) exhibited an ascending trend with the increase in water content and nozzle pressure, but started to decline when the nozzle pressure reached 0.70MPa due to air dehumidification. The total heat transfer (Q_z) was in balance at first and then decreased.

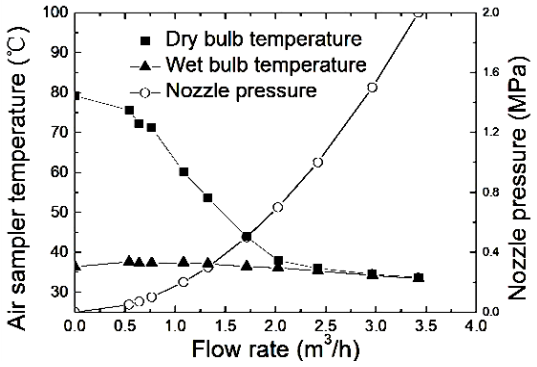

Fig. 3. Variation in the air sampler temperature in 1/2 TF6 WC2

The spray cooling was mainly driven by evaporative cooling before the saturation of the air. The dominant driving force shifted to heat convection between the air and water at the nozzle pressure of 0.70MPa. As far as water saving is concerned, evaporative cooling should be the primary driving force of spray cooling. The inapparent decrease of dry-bulb temperature at the nozzle pressure of 0.70MPa demonstrates that 0.70MPa is the critical pressure for spray cooling of TF6 nozzle. In other words, the decline of dry-bulb temperature will not be accelerated by any further increase in nozzle pressure beyond 0.70MPa.

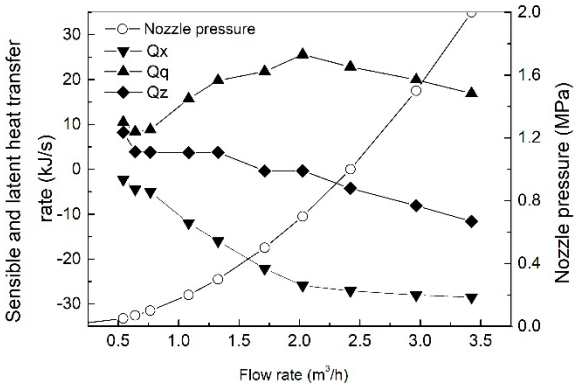

Fig. 4. Heat transfer and mass transfer in 1/2 TF6 WC2

4.2. Energy balance in droplet atomization

The critical nozzle pressure (0.7MPa) was further explained based on the energy balance during droplet atomization. The control volume of the water in the nozzle (hereinafter referred to CV1) and the control volume of the jet flow out of the nozzle (hereinafter referred to as CV2) were confirmed to facilitate the theoretical analysis. The CV1 is depicted by the dash line in Fig. 5.

The volume, surface area and mass of the nozzle are denoted as V (m^3), S (m^2) and m_l (kg), respectively; For CV1, the nozzle pressure and the flow velocity are denoted as P (Pa) and u_1 (m/s), respectively; For CV2, the nozzle pressure is equal to

the ambient pressure P_0 (Pa), and the flow velocity is denoted as u_2 (m/s).

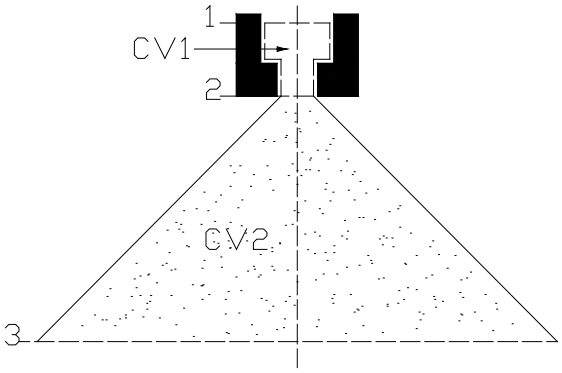

Fig. 5. Diagram of control volume

For CV1, there exists the following energy balance relationship (Eq. 6):

$$p + \frac{1}{2}\rho u_1^2 = P_0 + \frac{1}{2}\rho u_2^2 + P_{lose1-2} \tag{6}$$

Since the pressure loss $P_{lose1\text{-}2}$ in the working condition and $1/2\rho u_1^2$ in the above expression are so small as to be negligible, the above expression can be simplified as given by Eq. (7).

$$P = P_0 + \frac{1}{2}\rho u_2^2 \tag{7}$$

Thus, the jet velocity of the water at the nozzle outlet can be obtained as given by Eq. (8).

$$u_2 = \sqrt{\rho \frac{2(P - P_0)}{}} = \sqrt{\frac{2\Delta P}{\rho}} \tag{8}$$

During the experiment, the spray water flow rate and nozzle pressure (Table 1) were measured. And the nozzle flow characteristic l=3.18×$\Delta P^{1/2}$ was found through data fitting. Where l is the spray rate of the single nozzle (l/min), the unit of ΔP is 0.1MPa and the jet velocity could be calculated from l and the nozzle geometry, which supported the neglection of the two terms ($P_{lose1\text{-}2}$ and $1/2\rho u_2$).

The CV2 refers to the jet flow out of the nozzle, including droplets formed and the air entrained by these droplets after atomization. Assuming that the water has broken into droplets with a uniform diameter of d within t(s) after leaving the nozzle (i.e. moving from control surface 2 to control surface 3), the surface area, average velocity and mass of the spray are respectively S_{drop}, u_{drop} and m_{drop} at that moment. Other assumptions are as follows. Suppose that the pressure at control surface 3 equals the ambient pressure of P_0 (Pa), that the air entrained by the spray from the still air environment has a mass of m_a (kg) and a velocity consistent with that of the droplets u_{drop} (m/s), and that the surface tension coefficient, dynamic viscosity coefficient and density of the water are σ (N/m), μ (N/sm^2) and ρ_l (kg/m^3), respectively.

For CV2, the total energy required to atomize the water with a volume of V is given by Eq. (9).

$$E = \Delta PV = (P - P_0)V = \frac{1}{2} m_l u_2^2 \tag{9}$$

During atomization, the work to overcome water tension is given by Eq. (10).

$$W_\sigma = \sigma \Delta S = \sigma (S - \sum S_{drop}) \tag{10}$$

The viscous dissipation work, i.e. the work to overcome water viscosity is given by Eq. (11).

$$W_\mu = \int_V \int_t \Phi dV dt \tag{11}$$

where Φ is the viscous dissipation work of water per unit volume in a unit of time. According to the previous research (Clark, 1988; Ibrahim et al., 1993; Liu and Reitz, 1997), viscous dissipation work mainly occurs in the deformation of droplets, and is negligible in water atomization.

The kinetic energy of water droplets is given by Eq. (12).

$$W_{drop} = \frac{1}{2} \sum m_{drop} u_{drop}^2 \tag{12}$$

The water mass should be equal before and after atomization as is given by Eq. (13).

$$m_i = \sum m_{drop} \tag{13}$$

Hence, Eq. 12 can be rewritten as given by Eq. (14).

$$W_{drop} = \frac{1}{2} m_i u_{drop}^2 \tag{14}$$

The kinetic energy of the air entrained by droplets is given by Eq. (15).

$$W_{air} = \frac{1}{2} \sum m_a u_{drop}^2 \tag{15}$$

Without considering any mechanical loss, the energy balance during atomization is given by Eq. (16).

$$E = W_\sigma + W_\mu + W_{drop} + W_{air} \tag{16}$$

The kinetic energy of the air in Eq. 16 is also negligible, because the volume of the air entrained by droplets in such a short distance is fairly small compared with the water flow (Sutherland et al., 1997). Therefore, the energy balance can be expressed by Eq. (17).

$$E = W_\sigma + W_\mu + W_{drop} \quad (17)$$

The results show that all atomization energies but the kinetic energy of droplets were used to overcome the surface tension and viscosity of the water during the atomization.

4.3 Atomization features of TF6 nozzle

According to the results measured by Malvern Spraytec, a curve was plotted for the variation in diameter of atomized droplets of the TF6 nozzle at the nozzle pressure of *P* in Fig. 6. The data were measured 7cm below the nozzle. The diameters are denoted as $D_{[3][2]}$, $D_{[4][3]}$, $D_{v(10)}$, $D_{v(50)}$ and $D_{v(90)}$.

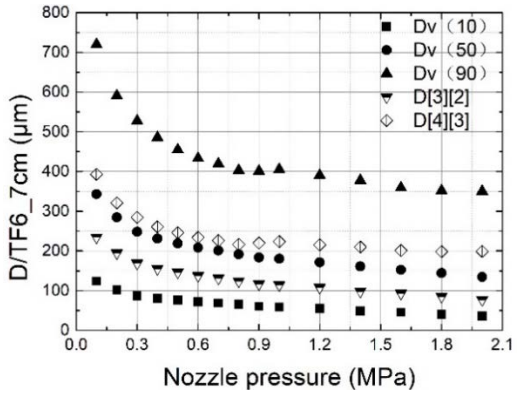

Fig. 6. Variation in diameter of atomized droplets of TF6 nozzle with nozzle pressure

The distribution law of atomized droplet diameters was summarized based on Fig. 6. The diameters, sorted in descending order, are $D_{v(90)}$, $D_{[4][3]}$, $D_{v(50)}$, $D_{[3][2]}$ and $D_{v(10)}$. With the increase in nozzle pressure, the diameters of atomized droplets reduced to a limited extent. After the TF6 nozzle pressure reached 0.70MPa, the atomized droplets showed inapparent changes in diameter. This means 0.70MPa is the critical value of the nozzle pressure for TF6 nozzle. In other words, the decline of droplet diameter will not be accelerated by simply increasing the nozzle pressure beyond 0.70MPa. The type of nozzle must be replaced to produce a finer water spray.

According to the energy balance analysis of the atomization process, the kinetic energy at control surface 2 (Fig. 5) was mainly consumed to overcome the surface tension and viscous forces before the nozzle pressure reaches 0.70MPa. In this case, the nozzle pressure is positive correlation with the work needed to overcome the surface tension and viscous forces, and negative correlation with droplet diameter. Due to the decrease in the droplet diameter, the surface area of the air-water interface expanded, which facilitates the heat and mass transfer between atomized droplets and the air. The relationship between nozzle pressure and the surface area rate of droplets is shown in Fig. 7. After the nozzle pressure reached 0.70MPa, the diameter of atomized droplet $D_{[3][2]}$ was 130.9μm，while the droplet surface area rate was 6.4223m^2/s. And the variation in $D_{[3][2]}$ was not obvious, and the work needed to overcome the surface tension and viscous forces was essentially invariable. At this moment, the balance energy in control surface 2 was converted into the kinetic energy of the water spray. The increase in nozzle pressure caused gradual growth of droplet velocity, which, in turn, shortened the contact time between water and the air. The situation is not conducive to the exchange of heat and moisture.

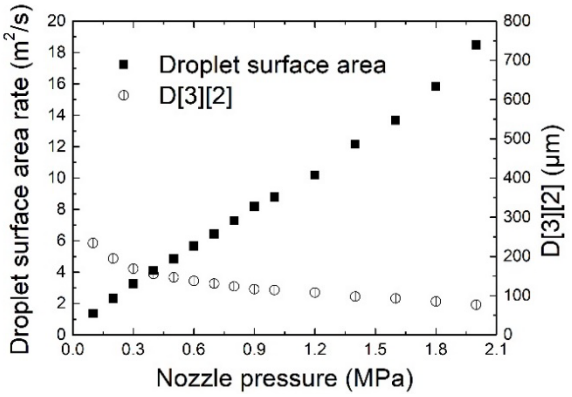

Fig. 7. The relationship between nozzle pressure and droplet surface area rate

5. Discussions

5.1. Fitting correlation of cooling effect

When evaporative cooling is the main cooling mechanism, the decline of dry-bulb temperature decrease in the air sampler is primarily motivated by the difference between dry-bulb and wet-bulb temperatures. Thus, the wet-bulb temperature at the inlet of the air sampler was taken as the cooling limit. In all the seven working conditions under 1/2 TF6, the same trend was observed (Fig. 8).

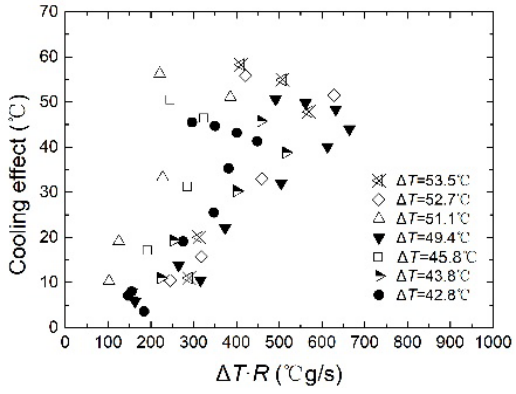

Fig. 8. Cooling effect vs. $\Delta T \cdot R$

First, the cooling effect, i.e. the decrease in dry-bulb temperature, was enhanced uniformly with the increase in the product of dry-wet bulb temperature difference ΔT and vaporization rate R ($\Delta T \cdot R$). When $\Delta T \cdot R$ reached a certain value, $\Delta T \cdot R$ decreased due to

air dehumidification while the cooling effect was still being enhanced.

The above phenomena indicate that the air temperature decrease was mainly driven by evaporative cooling before $\Delta T \cdot R$ reaches the certain value, but was replaced by heat convection when $\Delta T \cdot R$ exceeded that value. For this reason, the data acquired from this experiment should be fitted individually.

After fitting the data in the phase dominated by evaporative cooling, the relationship between the cooling effect ΔT_{db} and the product of ΔT and the spray rate L ($\Delta T \cdot L$) was obtained, as expressed by Eq. (18).

$$\Delta T_{db} = 60.08 \ln(\Delta T \cdot L + 52.89) - 254.46$$
$$23.17 \le \Delta T \cdot L \le 106.75 \quad (18)$$

where, ΔT is the dry-wet bulb temperature difference (°C); L is the spray rate (m^3/h). In this fitting correlation, ΔT represents the limit of the cooling effect and L is related to droplet surface area. Thus, the equation is physically meaningful. The relevant fitting coefficient R_2=0.94343, an evidence to the reliability of the fitting result (Fig. 9).

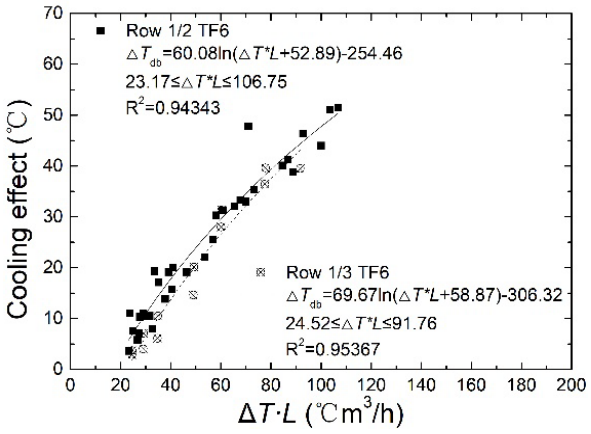

Fig. 9. Comparison of cooling effects

5.2 Comparison of cooling effects

In the first working condition of 1/3 TF6 (hereinafter referred to as 1/3 TF6 WC1), the air sampler temperature, heat transfer and mass transfer varied in a similar way to those in 1/2 TF6 WC2. Similarly, the relationship between the cooling effect ΔT_{db} and $\Delta T \cdot L$ in this working condition can be fitted as given by Eq. (17).

$$\Delta T_{db} = 69.67 \ln(\Delta T \cdot L + 58.87) - 306.32$$
$$24.52 \le \Delta T \cdot L + 58.87) - 306.32 \quad (17)$$

The relevant fitting coefficient R^2=0.95367, revealing the reliability of the fitting result (Fig. 9). Through the comparison between 1/2 TF6 WC2 and 1/3 TF6 WC1 (Fig. 9, Eq. 18, Eq. 19), it is learned that the cooling effect of 1/2 TF6 WC2 (row spacing: 500mm) is better than that of 1/3 TF6 WC1 (row spacing: 1,000mm) under the condition of the same $\Delta T \cdot L$.

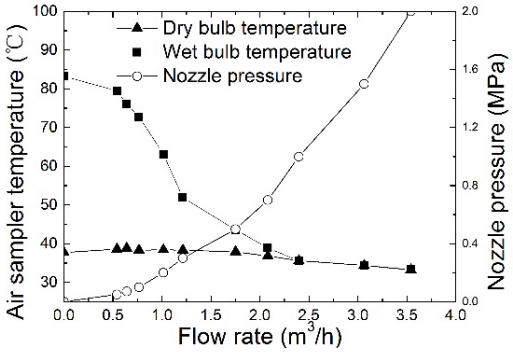

Fig. 10. Variation in air sampler temperature of 1/3 TF6 WC1

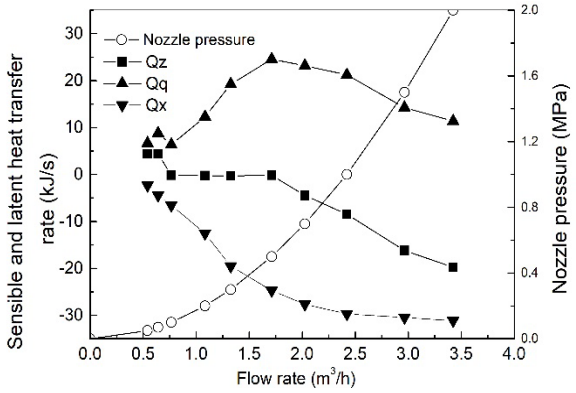

Fig. 11. Heat and mass transfers of 1/3 TF6 WC1

5.3 Error analysis

According to the Lewis correlation, the air side heat transfer rate Q_a is:

$$Q_a = M_{da}(h_{ao} - h_{ai}) = V_a \rho_a \Delta h_a \quad (20)$$

where V_a is the air volume flow; ρ_a is the dry air density. Then, the air side maximum relative error is:

$$E_{Q_a} = \pm \frac{V_a \rho_a |\delta \Delta h_a| + V_a \Delta h_a |\delta \rho_a| + \rho_a \Delta h_a |\delta V_a|}{V_a \rho_a \Delta h_a}$$
$$= \pm \left(\frac{|\delta \Delta_a|}{\Delta h_a} \right) + \left(\frac{|\delta \rho_a|}{\rho_a} \right) + \left(\frac{|\delta V_a|}{V_a} \right) \quad (21)$$

The maximum relative error E_{Qa} of the air side heat transfer rate Q_a equals the sum of the maximum relative error of the enthalpy difference $|\delta \Delta h_a|/\Delta h_a$, the maximum relative error of the dry air density $|\delta \rho_a|/\rho_a$ and the maximum relative error of the air volume flow $|\delta V_a|/V_a$.

For accurate calculation, the parameters are configured as follows: indoor temperature T_0=31.5°C; inlet air dry-bulb temperature T_1=35.1°C; inlet wet-bulb temperature $T_{1,s}$=28.1°C; outlet air dry-bulb temperature T_2=42.2°C; wet-bulb temperature $T_{2,s}$=38.7°C; wind velocity 6.1 m/s. In light of these parameters, the following can be calculated: the maximum relative error of the air side enthalpy

difference $E_{\Delta h}$=±4.02%, the maximum relative error of dry air density $E_{\rho a}$=±0.149%, and the maximum relative error of wet air volume flow E_{Va}=±0.78%. The three maximum relative errors were combined to derive the maximum relative error of the air side: E_{Qa}=±4.949%.

The error analysis proves the reliability of the experimental instruments and methods, and validates the effectiveness of the experimental results.

5. Conclusions

An experimental study about the spray cooling performance in a humidification chamber was conducted. During the experiment, the spray cooling performance and atomization features were examined, and the cooling effects of different nozzle layouts were compared.

(1) The same trend was observed in all of the seven working conditions under 1/2 TF6 and both the two working conditions under 1/3 TF6: the dry-bulb temperature reached the wet-bulb temperature when the nozzle pressure reached 0.7MPa, whereas the decrease in air sampler temperature was not obvious despite further increase in nozzle pressure. The phenomena suggest that there is a critical pressure when the spraying cooling is mainly driven by evaporative cooling. It is useless to increase the spray pressure beyond that threshold.

(2) With the increase in nozzle pressure, the diameters of atomized droplets reduced to a limited extent. The variation law can be explained by the energy balance relationship in droplet atomization. Before the nozzle pressure reached 0.70MPa, the surface area of the air-water interface expanded, which facilitates the heat and mass transfer between atomized droplets and the air. The increase in nozzle pressure caused gradual growth of droplet velocity, which, in turn, shortened the contact time between water and the air. The situation is not conducive to the exchange of heat and moisture.

(3) After fitting the data in the phase dominated by evaporative cooling, the author obtained the relationship between the cooling effect ΔT_{db} and ΔTL under both 1/2 TF6 and 1/3 TF6, and acquired the applicable range of the fitting correlation. The relevant fitting coefficient manifested the reliability of the fitting results.

(4) Through the comparison between 1/2 TF6 WC2 and 1/3 TF6 WC1, it is learned that the cooling effect of 1/2 TF6 WC2 (row spacing: 500mm) is superior to that of 1/3 TF6 WC1 (row spacing: 1,000mm) under the condition of the same $\Delta T{\cdot}L$.

This research discovered the critical pressure and optimal layout of TF6 nozzle in the humidification chamber. The experimental methods, analysis modes and fitting equations are suitable for analysing other nozzles like TF8 and AM4. Based on the existing research on nozzle flow features, the atomization features will be investigated using Malvern Spraytec, seeking to determine the critical parameters in a humidification chamber. Moreover, the experimental setup and mathematical model in the air cooler section will be built to optimize the whole spray humidification air cooler.

Acknowledgements

The authors gratefully acknowledge the support provided by the Jiangsu postdoctoral scientific research fund program and the scientific research fund of Nanjing Institute of Technology under grant no. CKJA201803.

References

Atreya A., Crompton T., Suh J., (1999), A study of the chemical and physical mechanisms of fire suppression by water, *Fire Safety Science Proceedings*, **6**, 493-504.

Back G.G., Beyler C.L., Hansen R. (2000), The capabilities and limitations of total flooding, water mist fire suppression systems in machinery space applications, *Fire Technol*, **36**, 8-23.

Bal S., Mishra P.C., Satapathy A.K., (2018), Optimization of spray parameters for effective microchannel cooling using surface response methodology, *International Journal of Heat and Technology*, **36**, 973-980.

Bishnoi P., Sinha M.K., (2018), Influence of the wettability nature of the nozzle wall on the dynamics of drop formation, *International Journal of Heat and Technology*, **36**, 1005-1009.

Camaraza-Medina Y., Rubio-Gonzales Á.M., Cruz-Fonticiella O.M., García-Morales O.F., (2018), Simplified analysis of heat transfer through a finned tube bundle in air cooled condenser, *Mathematical Modelling of Engineering Problems*, **5**, 237-242.

Camaraza-Medina Y., Rubio-Gonzales Á.M., Cruz-Fonticiella O.M., García-Morales O.F., Vizcón-Toledo R., Quiza-Sardiñas R., (2018), Simplified analysis of heat transfer through a finned tube bundle in air cooled condenser-second assessment, *Mathematical Modelling of Engineering Problems*, **5**, 365-372.

Chen C.W., Yang C.Y., Hu Y.T., (2013), Heat transfer enhancement of spray cooling on flat Aluminum tube heat exchanger, *Heat Transfer Engineering*, **34**, 29-36.

Clark M.M., (1988), Drop breakup in a turbulent flowi, conceptual and modelling considerations, *Chemical Engineering Science*, **43**, 671-679.

Dai Y., Wu W., Zhou H.B., Zhang J., Ma F.Y., (2018), Numerical simulation and optimization of oil jet lubrication for rotorcraft meshing gears, *International Journal of Simulation Modelling*, **17**, 318-326

Grant G., Brenton J., Drysdale D., (2000), Fire suppression by water sprays, *Progress in Energy and Combustion Science*, **26**, 79-130.

Hansen R.L., Back G.G., (2001), Water Spray Protection of Machinery Spaces, *Fire Technology*, **37**, 317-326.

Ibrahim E.A., Yang H.Q., Przekwas A.J., (1993), Modelling of spray droplets deformation and breakup, *Journal of Propulsion Power*, **9**, 651-654.

Jones A., Nolan P.F., (1995), Discussions on the use of fine water sprays or mists for fire suppression, *Journal of Loss Prevention in the Process Industries*, **8**, 17-22.

Jukka V., (2002), A transient one-zone computer model for total flooding water mist fire suppression in ventilated enclosures, *Fire Safety Journal*, **37**, 229-257.

Keramida E.P., Karayannis A.N., Boudouvis A.G., (2000), Numerical modelling of radiant heat attenuation through water mist, *Combustion Science and Technology*, **159**, 351-371.

Kutscher C., Costenaro D., (2002), Assessment of Evaporative Cooling Enhancement Methods for Air-

Cooled Geothermal Power Plants, *Transactions-Geothermal Resources Council*, 775-780.

Lefebvre A.H., (1989), *Atomization and Sprays*, Hemisphere Publishing Corporation, New York, 1989.

Lentati A.M., Chelliah H.K., (1998), Physical, thermal, and chemical effects of fine-water droplets in extinguishing counterflow diffusion flames, *Symposium (International) on Combustion*, **27**, 2839-2846.

Li H.X., Li B., Choi J., Heo J., Kim I., (2016), Analysis of a novel nozzle used for pulse jet filtration using CFD simulation method, *International Journal of Simulation Modelling*, **15**, 262-274.

Li G.R., Ge Y.F., Zheng Y., Xue X.Q., (2015), The research of stress theoretical analysis and structural parameters of sprayer fluid of rotating conical abrasive jet, *International Journal of Heat and Technology*, **33**, 33-40.

Liu Z., Reitz R.D., (1997), An analysis of the distortion and breakup mechanisms of high speed liquid drops, *International Journal of Multiphase Flow*, **23**, 631-650.

Lorenzini G., (2006), Water droplet dynamics and evaporation in an irrigation spray, *Transactions of the ASABE*, **49**, 545-549.

Lorenzini G., Saro O., (2013), Thermal fluid dynamic modelling of a water droplet evaporating in air, *International Journal of Heat and Mass Transfer*, **62**, 323-335.

Lorenzini G., Saro O., (2016), Analysis of water droplet evaporation through a theoretical-numerical model, *International Journal of Heat and Technology*, **34**, S189-S198.

Prasad K., Ll, C., Kailasanath K., Ananth R., (1998), Numerical modeling of fire suppression using water mist. 1, gaseous methane-air diffusion flames, *DTIC Document*.

Prasad K., Patnaik G., Kailasanath K., (2002), A numerical study of water-mist suppression of large scale compartment fires, *Fire Safety Journal*, **37**, 569-589.

Sardqvist S., Holmstedt G., (2001), Water for manual fire suppression, *Journal of Fire Protection Engineering*, **11**, 209-231.

Shimizu H., Tsuzuki M., Yamazaki Y., (2001), Experiments and Numerical Simulation On Methane Flame Quenching by Water Mist, *Journal of Loss Prevention in the Process Industries*, **14**, 603-608.

Sutherland J.J., Sojka P.E., Plesniak M.W., (1997), Entrainment by Ligament-Controlled Effervescent Atomizer-Produced Sprays, *International Journal of Multiphase Flow*, **23**, 865-884

Wrachien D.D., Lorenzini G., (2012), Quantum mechanics applied to the dynamic assessment of a cluster of water particles in sprinkler irrigation, *Journal of Engineering Thermophysics*, **21**, 193-197.

Wu J.R., Qi L.B., (2001), China's power industry development problem from 2001 to 2020, *Power System Technology*, **25**, 46-51.

Zeng Z., Sadeghpour A., Ju Y.S., (2019), A highly effective multi-string humidifier with a low gas stream pressure drop for desalination, *Desalination*, **449**, 92–100.